Original Article | Cardiovascular Imaging

eISSN 2005-8330
https://doi.org/10.3348/kjr.2020.0020
Korean J Radiol 2020;21(10):1165-1177

Korean Journal of Radiology
KJR

Incremental Image Noise Reduction in Coronary CT Angiography Using a Deep Learning-Based Technique with Iterative Reconstruction

Jung Hee Hong, MD[1], Eun-Ah Park, MD, PhD[1], Whal Lee, MD, PhD[1], Chulkyun Ahn, MD[2], Jong-Hyo Kim, MD, PhD[1, 2]

[1]Department of Radiology, Seoul National University College of Medicine, Seoul National University Hospital, Seoul, Korea; [2]Department of Transdisciplinary Studies, Graduate School of Convergence Science and Technology, Seoul National University, Seoul, Korea

Objective: To assess the feasibility of applying a deep learning-based denoising technique to coronary CT angiography (CCTA) along with iterative reconstruction for additional noise reduction.

Materials and Methods: We retrospectively enrolled 82 consecutive patients (male:female = 60:22; mean age, 67.0 ± 10.8 years) who had undergone both CCTA and invasive coronary artery angiography from March 2017 to June 2018. All included patients underwent CCTA with iterative reconstruction (ADMIRE level 3, Siemens Healthineers). We developed a deep learning based denoising technique (ClariCT.AI, ClariPI), which was based on a modified U-net type convolutional neural net model designed to predict the possible occurrence of low-dose noise in the originals. Denoised images were obtained by subtracting the predicted noise from the originals. Image noise, CT attenuation, signal-to-noise ratio (SNR), and contrast-to-noise ratio (CNR) were objectively calculated. The edge rise distance (ERD) was measured as an indicator of image sharpness. Two blinded readers subjectively graded the image quality using a 5-point scale. Diagnostic performance of the CCTA was evaluated based on the presence or absence of significant stenosis (≥ 50% lumen reduction).

Results: Objective image qualities (original vs. denoised: image noise, 67.22 ± 25.74 vs. 52.64 ± 27.40; SNR [left main], 21.91 ± 6.38 vs. 30.35 ± 10.46; CNR [left main], 23.24 ± 6.52 vs. 31.93 ± 10.72; all $p < 0.001$) and subjective image quality (2.45 ± 0.62 vs. 3.65 ± 0.60, $p < 0.001$) improved significantly in the denoised images. The average ERDs of the denoised images were significantly smaller than those of originals (0.98 ± 0.08 vs. 0.09 ± 0.08, $p < 0.001$). With regard to diagnostic accuracy, no significant differences were observed among paired comparisons.

Conclusion: Application of the deep learning technique along with iterative reconstruction can enhance the noise reduction performance with a significant improvement in objective and subjective image qualities of CCTA images.

Keywords: *Coronary artery disease; Multidetector computed tomography; Computed tomography angiography; Deep learning*

INTRODUCTION

The evolution of the computed tomography (CT) technology has led to an increase in the accuracy of coronary CT angiography (CCTA). Thus, CCTA has been used widely as a non-invasive alternative to invasive coronary angiography to exclude coronary artery disease (1, 2). The increased use of CCTA has led to concerns regarding an increase in the use of ionizing radiation and potential carcinogenesis over a person's lifetime. Therefore, the need for achieving a low radiation dose has increased.

In the past few decades, advances in CT technology, including new image acquisition and reconstruction algorithms such as iterative reconstruction, low tube voltage, and prospective electrocardiogram (ECG)-triggered axial high-pitch scans, have been made; these

Received: September 24, 2019 **Revised:** March 19, 2020
Accepted: March 20, 2020
Corresponding author: Eun-Ah Park, MD, PhD, Department of Radiology, Seoul National University College of Medicine, Seoul National University Hospital, 101 Daehak-ro, Jongno-gu, Seoul 03080, Korea.
• E-mail: iameuna1@gmail.com

advances resulted in a reduction in the radiation dose by approximately 78% (from 885 to 195 mGy*cm) from 2007 to 2017 (3-7). However, further reductions in radiation dose results in the degradation of image quality, mainly because of an increase in image noise. Increased image noise can compromise the diagnostic information of CT images. Therefore, much effort has been made to design better image processing techniques that can further reduce image noise.

Recently, the application of deep learning techniques to medical imaging has rapidly increased and is considered a promising solution to this problem. Especially with regard to CT denoising application, deep learning techniques have shown impressive performance in improving the imaging quality by image noise suppression, structural preservation, and lesion detection over the conventional filtered back projection (FBP) (8, 9).

In this study, we hypothesized that the application of deep learning technique could allow for an additional reduction in image noise on the CCTA images reconstructed with an iterative reconstruction technique. We aimed to assess the feasibility of applying a deep learning-based denoising technique to CCTA along with iterative reconstruction for additional noise reduction.

MATERIALS AND METHODS

This retrospective study was approved by the Institutional Review Board (IRB), and the requirement for informed consent was waived (IRB Number H1808-113-968).

Study Population

This study retrospectively evaluated the medical records of 82 consecutive adult patients (male:female, 60:22; mean age, 67.0 ± 10.8 years; age range, 25.0–85.0 years) who had undergone both CCTA and invasive coronary artery angiography with a time interval of less than 2 months (mean time interval, 11 ± 10 days; range, 0–36 days) from March 2017 to June 2018 at a single tertiary institution. Those patients who previously underwent coronary artery bypass surgery or percutaneous coronary artery intervention were excluded. Patients were enrolled regardless of CCTA image quality.

CT Scanning Protocol

CCTA images of all patients were acquired using a third generation 192-section dual-source CT scanner (SOMATOM Force, Siemens Healthineers).

For patients with a heart rate of less than 70 beats per minute (bpm), we used a prospectively ECG-triggered data acquisition method with very high pitch values in one heartbeat (FLASH protocol). The acquisition window was applied at a 70% R-R interval. For patients with a heart rate of over 70 bpm, we applied either prospective ECG-triggered sequential mode with 40% R-R interval or retrospective ECG-gated spiral mode with ECG pulsing.

Patients with a heart rate of over 65 bpm were administered 50–100 mg of oral metoprolol (Betaloc, AstraZeneca) 45–60 minutes prior to the CT examination, except in the case of those with a contraindication for beta-blockers. Sublingual nitroglycerin (0.4 mg; Nitroquick, Ethex) was administered to 49 patients; however, this step was excluded for subjects who had a contraindication for nitroglycerin after the completion of calcium scoring scanning. In patients who underwent CT with the FLASH protocol, 70 mL of a nonionic contrast medium (iomeprol; Iomeron 400, Bracco Diagnostics) was injected into the antecubital vein at a rate of 4 mL/s, followed by 30 mL of a contrast-saline mixture in 20:80 ratio. The patients who underwent CT with a sequential protocol were injected 80 mL of a contrast medium and 30 mL of a contrast-saline mixture in 20:80 ratio by using a dual power injector (Stellant, MEDRAD).

The acquisition scan range was from the mid ascending aorta to below the cardiac apex in a cranio-caudal direction. Initiation of scanning was based on the bolus tracking method (CARE Bolus, Siemens Healthineers). The region of interest (ROI) was placed within the ascending aorta and the triggering threshold was set to 100 HU. Attenuation based automatic tube voltage selection (CARE KV, Siemens Healthineers), with the available tube setting from 70–150 kVp in 10 kV increments (reference, 100 kVp), and automated tube current modulation (CARE Dose4D, Siemens Healthineers), with the reference tube current setting of 300 mAs, were applied. The additional scanning parameters used were as follows: gantry rotation time, 250 ms; detector collimation, 192 x 0.6 mm; and matrix size, 512 x 512 pixels.

All the CCTA images were reconstructed with a slice thickness of 0.75 mm and an increment of 0.5 mm. Image data were rendered using a medium smooth (Bv40) reconstruction kernel with an iterative reconstruction technique (ADMIRE level 3, Siemens Healthineers).

https://doi.org/10.3348/kjr.2020.0020

Korean Journal of Radiology
KJR

Deep Learning-Based Denoising Technique

We developed a deep learning-based denoising technique (ClariCT.AI, ClariPI), which was based on a modified U-net type convolutional neural net (CNN) model (Fig. 1) (10). The conventional U-net architecture was modified to fit to the denoising purpose by reducing the number of convolution filters and applying batch-normalization (BN), which prevent overfitting while improving training stability (11, 12).

The model consisted of a contracting path and an expansive path, which were connected by a concatenated skip-connection. The contracting path applied a convolution layer with a 4 x 4 kernel size followed by a BN layer, a rectified linear unit activation (13), and 2 x 2 max-pooling layers. The expansive path was almost similar to the contracting path with the exception of the max-pooling layers that were replaced by 2 x 2 up-convolution layers to restore the spatial resolution. The weights and biases of the deep learning model were optimized using an Adam optimizer (14) in a TensorFlow framework (15).

For the training of the model, 55418 standard-dose prospective ECG-gated thoracic CT angiography (CTA) images of 100 patients were used. The scan parameters were as follows: tube voltage of 70–120 kVp, reference tube current setting of 300 mA, mean volume CT dose index ($CTDI_{vol}$) of 12.1 ± 6.7 mGy, slice thickness of 0.75 mm with iterative image reconstruction using ADMIRE level 3 and Bv40 kernel. A digital imaging and communication in medicine (DICOM)-based low-dose simulation tool was applied to generate a paired dataset of realistic low-dose CTA images (16) and synthetic noise component images. Varying degrees of low-dose simulations ranging from 50%-dose to 5%-dose levels of the original dose were applied to the CTA image set.

To match the reconstruction field of view (FOV) of the thorax CTA images to that of the CCTA images, the heart regions from the paired dataset were cropped and resized to a 512 x 512 matrix. Training of the CCTA denoising model was performed iteratively to minimize the difference between the ground-truth synthetic noise component images and the predicted noise images from the input noisy low-dose images.

In the final step of the denoising process, the trained deep learning model produced a predicted noise component image of the given noisy CCTA image, and then the noise component was scaled and subtracted from the noisy input CCTA image.

CT Image Analysis

Objective Image Assessment

To compare the objective image quality between the denoised and original CT images, four parameters, namely, image noise, CT attenuation, signal-to-noise ratio (SNR), and contrast-to-noise ratio (CNR) were analyzed for each dataset by a single reader, following the previously described methods (17, 18).

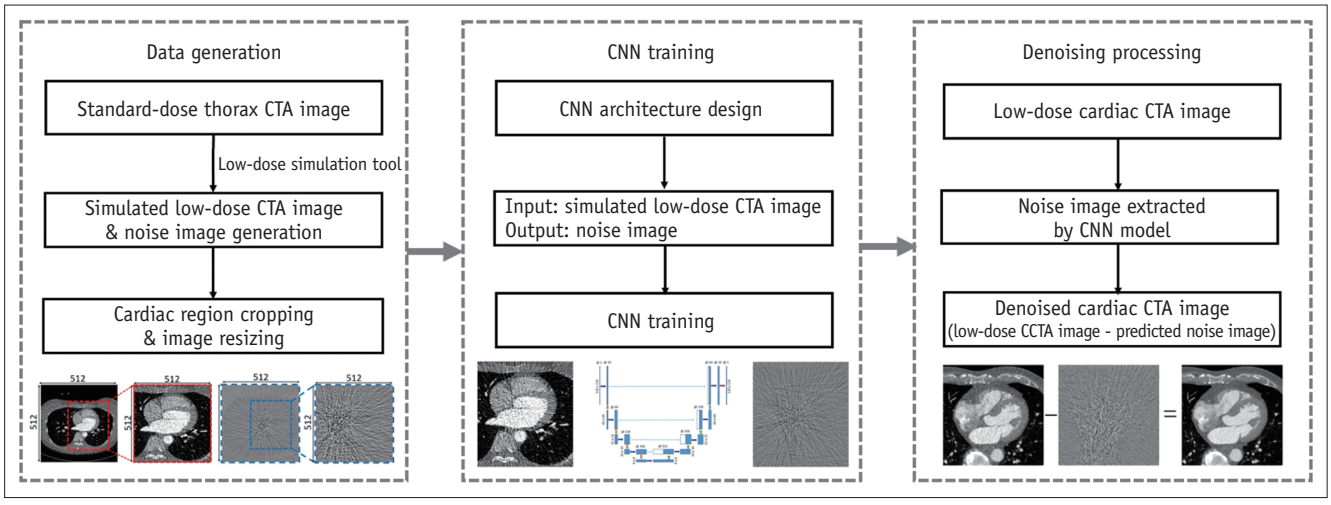

Fig. 1. Flow diagram of deep learning-based denoising algorithm. Figure shows overall procedure of deep learning-based cardiac CTA denoising algorithm. Low-dose simulation tool was applied to standard-dose thorax CTA images to generate set of simulated low-dose images, from which cardiac region was selected and rescaled to 512 x 512 matrix. Simulated low-dose CTA image set was fed into CNN model to train it such that model could extract noise component images from noisy input CTA images. Trained model extracted noise component image from real low-dose CCTA image, which was then subtracted from input image to produce denoised CCTA image. CCTA = coronary CT angiography, CNN = convolutional neural net, CTA = CT angiography

https://doi.org/10.3348/kjr.2020.0020

CT attenuation of the proximal and distal segments of the major coronary arteries (left main [LM], left anterior descending [LAD], circumflex [LCx], and right coronary arteries [RCAs]) was derived from the largest possible scaled ROIs within the first 5 mm of the segment (minimum size, more than 2 mm^2) while carefully avoiding the inclusion of the vessel wall and calcification. The image noise was defined as the standard deviation (SD) of the CT attenuation measured at the aortic root, cranial to the left coronary ostium (size, 300 mm^2). For the vessel contrast, the CT attenuation of the anterior chest wall adipose tissue was measured (size, 100 mm^2) (19). The ROIs were precisely placed at the same location for corresponding original and denoised images.

Consequently, the SNR and CNR used were calculated as follows:

SNR = (CT attenuation$_{\text{major coronary arteries}}$ / noise)

CNR = ([CT attenuation$_{\text{major coronary arteries}}$ - CT attenuation$_{\text{adipose tissue of chest wall}}$] / noise)

To evaluate the effect of a deep learning-based denoising technique on image sharpness in a quantitative manner, we additionally analyzed the edge rise distance (ERD) as an indicator of this parameter in original and denoised images. The ERD is defined as the distance required for the edge response to rise from 10% to 90% of the final pixel intensity. A smaller ERD indicates a higher sharpness of the images. To measure the ERD, we used proximal LAD as a main ROI. We drew short line segments perpendicular to the border of the artery. The edge-line profiles were extracted along the short-line segments, averaged, and plotted. We measured the maximum value of the plotted average edge-line profile. Finally, the ERD was calculated as the distance of pixel locations between the shoulder pixel, which corresponds to 90% of the maximum pixel intensity, and the tail pixel, which corresponds to 10% of the maximum pixel intensity (20). The ERD measurements were carried out by a single observer using a software programmed with MATrix LABoratory (MathWorks).

Subjective Image Assessment

Two independent and experienced readers (with 5 and 14 years of clinical experience in cardiac CT interpretation, respectively) who were blinded to the two groups of images (original vs. denoised images) independently reviewed the 164 data sets (82 original images and 82 denoised images); the obtained results were averaged for analysis. In addition, the investigators were not allowed to access data on indications for imaging, patient characteristics, and imaging reports. Each radiologist was allowed to change the window level and width as desired. Overall subjective image quality was evaluated in terms of the vessel wall definition with quantum noise on a 5-point scale as follows: 0 (non-diagnostic) = significant impairment in image quality because of excessive image noise; 1 (poor) = evident limitations in the vessel wall definition owing to poor contrast enhancement of the vessel lumen, blurring of the vessel wall, or severe image noise—acceptable only under limited conditions for the evaluation of a few proximal coronary arteries; 2 (good) = minimal limitations in the vessel wall definition owing to low contrast enhancement of vessel lumen, blurring of the vessel wall, or moderate image noise; 3 (very good) = well-preserved vessel wall definition with a good attenuation of the vessel lumen and minimal image noise; 4 (excellent) = clear vessel wall definition with excellent attenuation of the vessel lumen from the proximal to distal end and barely perceived image noise—fully acceptable for diagnostic interpretation (21, 22).

Coronary Artery Analysis Using CCTA

Diagnostic performance of the CCTA was determined by the same readers, who reviewed the coronary arteries while being blinded to details of CT dataset, independently. Using a 15-segment classification system of the coronary arteries (23), all evaluable coronary artery segments, including their side branches with a minimum diameter of at least 2.0 mm (total 1039 segments), were evaluated to determine the presence or absence of significant stenosis (≥ 50% reduction in lumen diameter). In case of inter-observer disagreement, each segment was re-evaluated consensually. Considering invasive coronary angiography as the reference standard, axial images were mainly used for comparing the diagnostic performance of the original and denoised CCTA for the evaluation of the coronary artery stenosis. Multiplanar reconstructions were obtained and evaluated to ascertain indeterminate lesions.

Subgroup Analysis according to the Acquisition Methods, Calcified Burden, and Coronary Vessel Size

To exclude the influence of the acquisition methods (FLASH, prospective or retrospective ECG gaiting) and the calcification burden of the coronary arteries on noise reduction, we performed subgroup analysis based on the acquisition method and the total Agaston score (0; 1–10; 11–100; 101–400; > 400) of the coronary arteries to

https://doi.org/10.3348/kjr.2020.0020

Korean Journal of Radiology
KJR

determine the diagnostic accuracy and objective (image noise, SNR and CNR) and subjective image qualities. Additionally, to investigate the diagnostic accuracy and image quality according to the coronary vessel size (proximal [pLAD, pRCA, pLCx, LM], middle [mLAD, mRCA], distal [dLAD, dRCA, dLCx], branch arteries [diagonal, posterior descending artery, ramus intermedius, obtuse marginal and posterolateral branch]), we performed subgroup analysis accordingly to determine the diagnostic accuracy. There were only two patients in the groups of Agaston score "0" and "1–10," thus, statistical analysis could not be performed in these two groups.

Invasive Coronary Angiography

Experienced cardiologists performed invasive coronary angiograms according to the standard protocol of our hospital. As for the reference, the severity of the stenosis was documented after an interpretation of at least two projections for each coronary artery using quantitative coronary analysis (QCA, version 3.3, Philips Healthcare).

Statistical Analysis

Paired, two-tailed Student's *t* test was used to assess whether there were significant differences in objective image quality between the original and denoised images. The Wilcoxon signed rank test was used to identify if a significant difference existed in the subjective image quality between the two groups. Cohen's kappa and intraclass correlation (ICC) statistics were used to assess the inter-observer agreement in subjective image analysis (0.81–1.00, excellent; 0.61–0.81, good; 0.41–0.60, moderate; 0.21–0.40, fair; and < 0.20, poor agreement). Average ERD was compared using paired, two-tailed Student's *t* test.

The diagnostic performance of CCTA was calculated based on accuracy, sensitivity, specificity, positive predictive value (PPV), negative predictive value (NPV), true positive, true negative, false positive, and false negative. We used the McNemar's test for identifying significant differences in the sensitivity and specificity between the two groups. Weighted generalized score statistics were used for the comparison of the PPV and NPV between the two groups.

A p value of < 0.05 was considered statistically significant. The two-tailed Student's *t* test, the Wilcoxon signed rank test, McNemar's test, and determination of Cohen's kappa were performed using SPSS software (SPSS for Windows, version 22.0, IBM Corp.). ICC and weighted generalized score statistics were determined using R statistical software (R version 3.5.1, http://www.R-project.org/.), "DTComPair" R package (version 1.0.3, published by Christian Stock), and "ICC" R package (version 2.3.0, published by Matthew Wolak) (24).

RESULTS

Patient demographics, CCTA, and radiation dose parameters are presented in Table 1. Median calcium score (Agaston score) was 263.9 (interquartile range, 57.9–1149.8). The CARE KV lead utility was of low tube potential, between 70 kVp and 90 kVp. The mean values of the $CTDI_{vol}$, dose length product, and effective dose were 8.79 ± 7.62 mGy, 144.54 ± 129.47 mGy*cm, and 2.03 ± 1.81 mSv, respectively.

Objective and Subjective Image Quality

Image noise significantly decreased from a mean of 67.22 ± 25.74 in the original images to 52.64 ± 27.40 in the denoised images (p < 0.001). Both segment-based SNR and CNR of denoised images were significantly higher than those of the original images. Proximal and distal SNR and CNR of the denoised images were also significantly higher (Table 2, Fig. 2).

The mean scores of the total subjective image quality were significantly better in the denoised images than in the original images (Table 2, Figs. 2-4). There were 34 cases (34/82, 41.5%) where the image quality scores improved by more than one point. Forty-four cases (44/82,

Table 1. Patient Demographics, CCTA, and Radiation Dose Parameters

Demographics and Radiation Dose	Data*
Age (years)	67.0 ± 10.8
Male/female	60/22
BMI (kg/m^2)	24.7 ± 3.4
Heart rate (bpm)	68.2 ± 14.8
Tube potential (70/80/90 kVp)	35/35/12
FLASH/prospective sequential mode/ retrospective spiral mode	28/20/34
Calcium score (Agaston score)†	263.9 (57.9–1149.8)
$CTDI_{vol}$ (mGy)	8.79 ± 7.62
DLP (mGy*cm)	144.5 ± 129.5
Effective dose (mSv)‡	2.03 ± 1.81

*Data are presented as mean ± SDs, †Median and quartiles, ‡Effective dose was calculated by multiplying DLP with conversion factor of 0.014 mSv/mGy*cm (44). BMI = body mass index, CCTA = coronary CT angiography, $CTDI_{vol}$ = volume CT dose index, DLP = dose length product, SD = standard deviation

https://doi.org/10.3348/kjr.2020.0020

Table 2. Result of Segment-Based SNR and CNR Measurement and Subjective Image Quality in Original and Denoised Images

Image Quality	Locations	Original	Denoised	ODD	*P**
		Mean ± SD	Mean ± SD	Mean ± SEM	
Objective quality	Aortic root noise	67.22 ± 25.74	52.64 ± 27.40	14.58 ± 0.20	< 0.001
Lumen density (HU)	Left main	697 ± 155	694 ± 155	3 ± 1	< 0.001
	Proximal LAD	623 ± 157	625 ± 160	-2 ± 1	0.056
	Proximal LCx	624 ± 148	630 ± 151	-7 ± 1	< 0.001
	Proximal RCA	646 ± 162	655 ± 167	-9 ± 1	< 0.001
	Distal LAD	449 ± 133	456 ± 138	-7 ± 1	< 0.001
	Distal LCx	480 ± 143	479 ± 152	-0 ± 2	0.874
	Distal RCA	601 ± 190	612 ± 195	-10 ± 1	< 0.001
SNR	Left main	21.91 ± 6.38	30.35 ± 10.46	-8.55 ± 0.51	< 0.001
	Proximal LAD	19.66 ± 6.53	27.53 ± 10.71	-7.95 ± 0.52	< 0.001
	Proximal LCx	14.21 ± 5.35	20.12 ± 8.53	-5.96 ± 0.40	< 0.001
	Proximal RCA	20.29 ± 6.44	28.63 ± 10.54	-8.43 ± 0.52	< 0.001
	Distal LAD	19.62 ± 6.05	27.68 ± 10.06	-8.24 ± 0.50	< 0.001
	Distal LCx	15.20 ± 5.81	21.29 ± 9.30	-6.14 ± 0.43	< 0.001
	Distal RCA	18.69 ± 6.70	26.49 ± 10.82	-7.88 ± 0.52	< 0.001
	Proximal segment	20.38 ± 6.39	28.56 ± 10.46	-8.18 ± 0.26	< 0.001
	Distal segment	18.60 ± 6.70	22.63 ± 9.95	-6.59 ± 0.26	< 0.001
CNR	Left main	23.24 ± 6.52	31.93 ± 10.72	-8.79 ± 0.53	< 0.001
	Proximal LAD	21.28 ± 6.67	29.63 ± 10.96	-8.42 ± 0.54	< 0.001
	Proximal LCx	17.04 ± 5.76	23.98 ± 9.22	-7.01 ± 0.45	< 0.001
	Proximal RCA	22.03 ± 6.57	30.95 ± 10.87	-9.01 ± 0.55	< 0.001
	Distal LAD	21.16 ± 6.11	29.69 ± 10.18	-8.71 ± 0.53	< 0.001
	Distal LCx	17.47 ± 6.22	24.20 ± 10.03	-6.81 ± 0.47	< 0.001
	Distal RCA	21.31 ± 7.27	30.47 ± 11.93	-9.25 ± 0.59	< 0.001
	Proximal segment	21.93 ± 6.49	30.56 ± 10.68	-8.62 ± 0.27	< 0.001
	Distal segment	18.61 ± 6.70	26.22 ± 10.84	-7.61 ± 0.30	< 0.001
Subjective quality		2.45 ± 0.62	3.65 ± 0.60	-1.10 ± 0.05	< 0.001

Data are presented as mean ± SDs. *p < 0.001 indicates significant finding. CNR = contrast-to-noise ratio, HU = Hounsfield units, LAD = left anterior descending, LCx = left circumflex, ODD = original-denoised difference, RCA = right coronary artery, SEM = standard error of mean, SNR = signal-to-noise ratio

53.7%) showed an improvement in image quality by one point, and only 4 cases (4/82, 4.9%) showed no image quality improvement. The inter-observer agreement for the subjective image quality in 164 data sets showed good agreement (Cohen's Kappa, 0.619; ICC, 0.751).

In the subgroup analysis based on the acquisition method and calcification burden, image noise was significantly reduced in all groups. Indeed, SNR, CNR, and subjective image quality were significantly higher in the denoised images than in the original images in all comparisons. However, the CT attenuation of the major coronary vessels showed inconsistent results between each comparison (Supplementary Tables 1-6).

In terms of the results of objective sharpness, the average ERDs of denoised images were significantly smaller than those of the originals, which means that the denoised images were sharper than the originals (original vs denoised images: 0.98 ± 0.08 vs. 0.90 ± 0.08, p < 0.001) (Figs. 3, 4).

Diagnostic Performance of the CCTA

Table 3 exhibits the diagnostic performance of the two groups. No significant difference was observed among paired comparisons (Figs. 3, 4). There was no significant difference in the diagnostic performance between the original and denoised images in the subgroup analysis (Supplementary Tables 7-16).

DISCUSSION

We have described a novel deep learning-based denoising technique, which was based on a modified U-net type CNN model designed to predict the low-dose noise occurring in

https://doi.org/10.3348/kjr.2020.0020

Korean Journal of Radiology
KJR

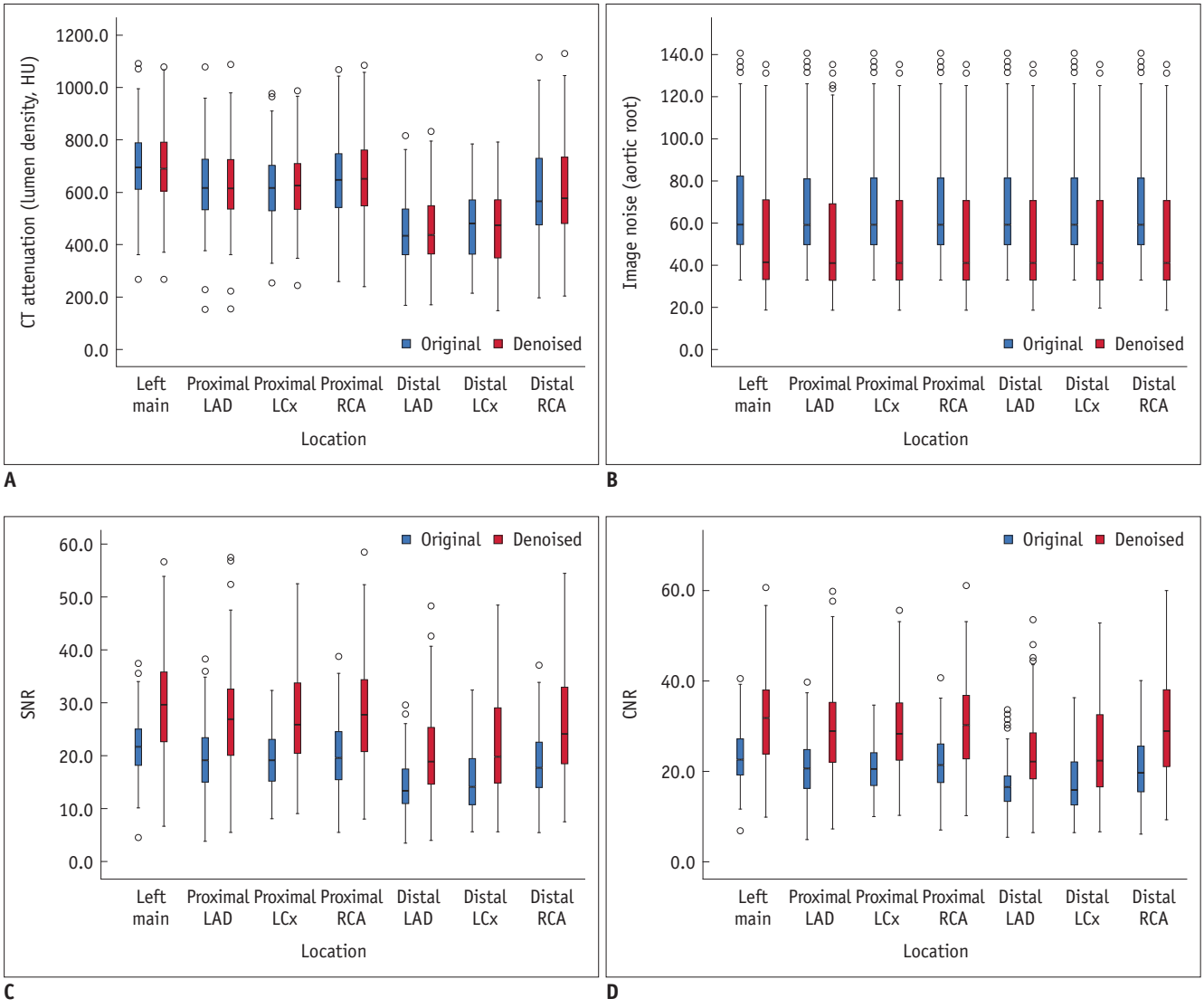

Fig. 2. Boxplots of objective measurements of both original and denoised images, according to four different protocols.
A. CT attenuation (lumen density, HU) of major coronary vessels (left main, LAD, LCx, RCA). **B.** Image noise of aortic root. **C.** Segment-based SNR. **D.** Segment-based CNR. Small circles indicate outliers. CNR = contrast-to-noise ratio, HU = Hounsfield units, LAD = left anterior descending, LCx = left circumflex, RCA = right coronary artery, SNR = signal-to-noise ratio

the originals. Our deep learning-based denoising technique used along with iterative reconstruction demonstrated a significant improvement in CCTA image quality, reduction in image noise by more than 20%, and increase in objective and subjective image qualities by approximately 40% without over-smoothing. Even after adjusting the acquisition method and calcification burden of coronary arteries, the denoised images still showed a significant image quality improvement over the originals.

This new deep learning-based approach has already been shown to reduce image noise even in ultra-low dose CCTA datasets, which were obtained using a tube current of 4% of the maximum ECG pulsing window (MinDose) in an experimental setting (10). In our study, we evaluated the image quality and diagnostic accuracy of CCTA performed with a low-dose CT using iterative reconstruction along with this deep learning-based denoising technique. Although there was no significant improvement in the diagnostic accuracy of the coronary artery stenosis, the proposed technique has achieved significant noise reduction with quantitative and qualitative improvement in image quality and good intra-observer agreement. Our paper verifies that the deep learning-based denoising technique could lead to an additional enhancement of image quality in a routine clinical setting of CCTA.

Unlike other studies investigating the performance of

https://doi.org/10.3348/kjr.2020.0020

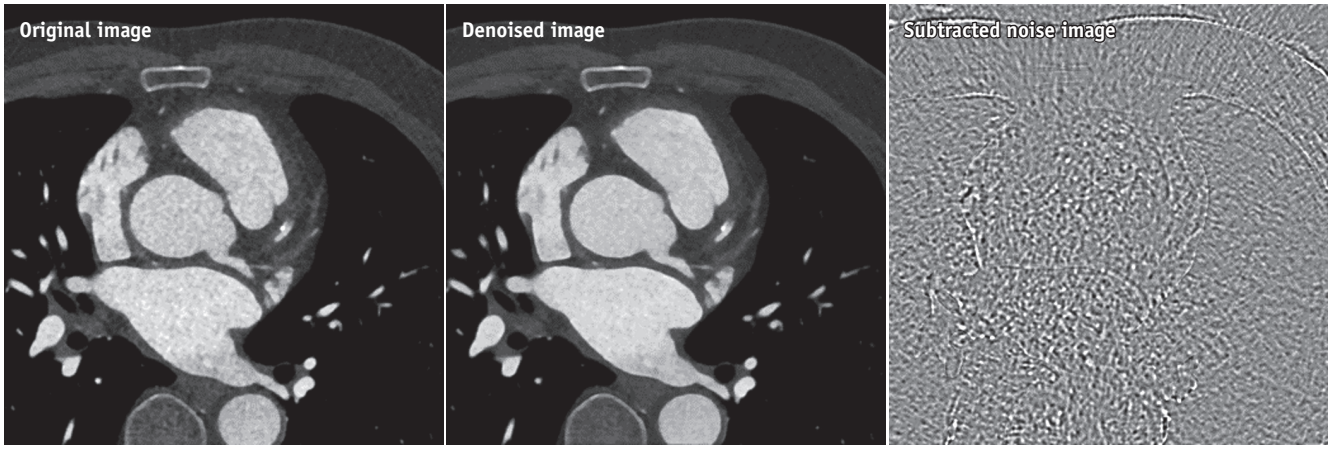

A

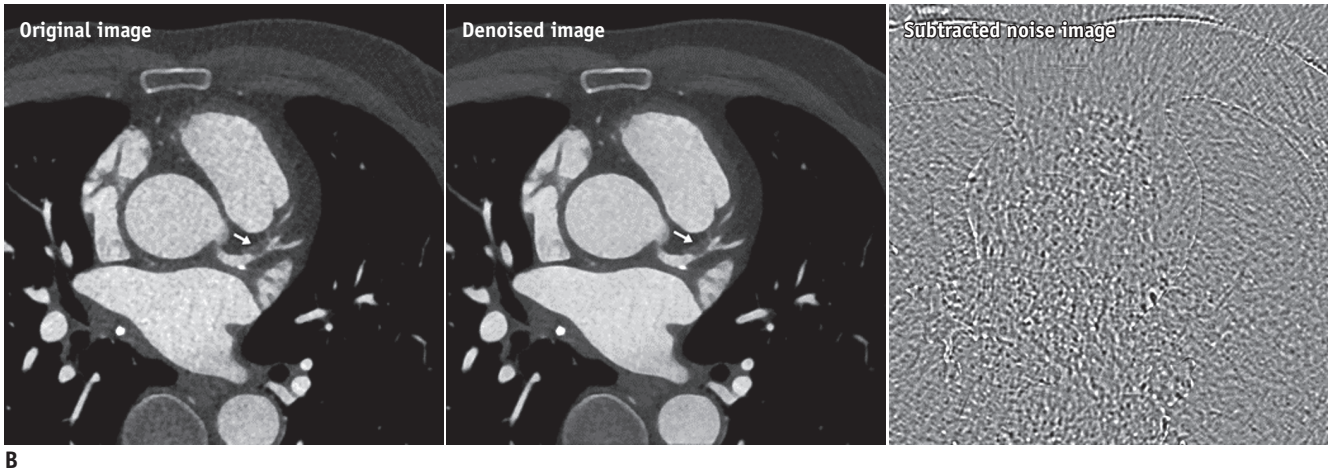

B

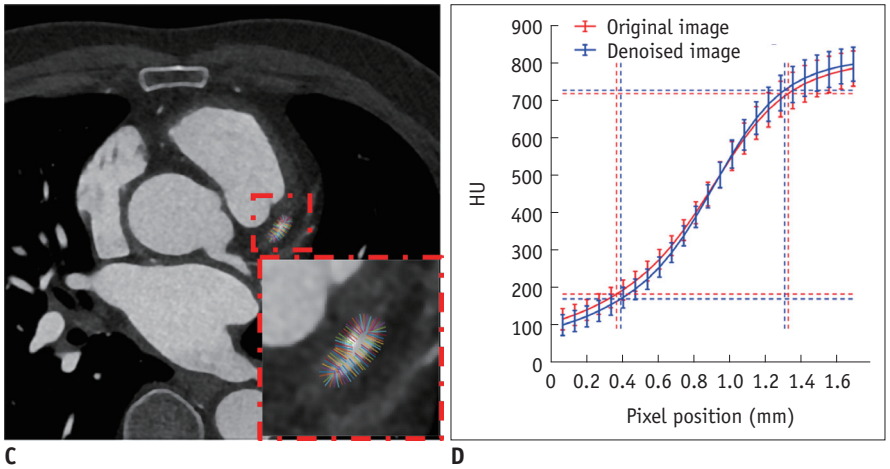

C

D

Fig. 3. CT images of 72-year-old male patient.
(A, B) Original axial CT scan, denoised CT images, and subtracted noise images, **(C)** example of analysis of ERD, and **(D)** graph showing results of ERD of original and denoised images. **A, B.** Denoised images are less noisy images that maintain sharp contour for visual evaluation of vessel structures; original images show moderate image noise. Noncalcified plaque (arrows) with high grade coronary artery stenosis of proximal LAD artery is well depicted on both images. **C.** Multiple short line segments were drawn perpendicular to border of artery with color overlay to calculate ERD. This example is shown on denoised image. **D.** Graph showing comparison of average CT number profiles along line segments of original and denoised images. Average ERD values are 0.9589 and 0.9141 for original and denoised images, respectively. ERD of denoised image is smaller than that of original image, indicating that denoised image is sharper than original image in objective criteria. ERD = edge rise distance

https://doi.org/10.3348/kjr.2020.0020

Korean Journal of Radiology
KJR

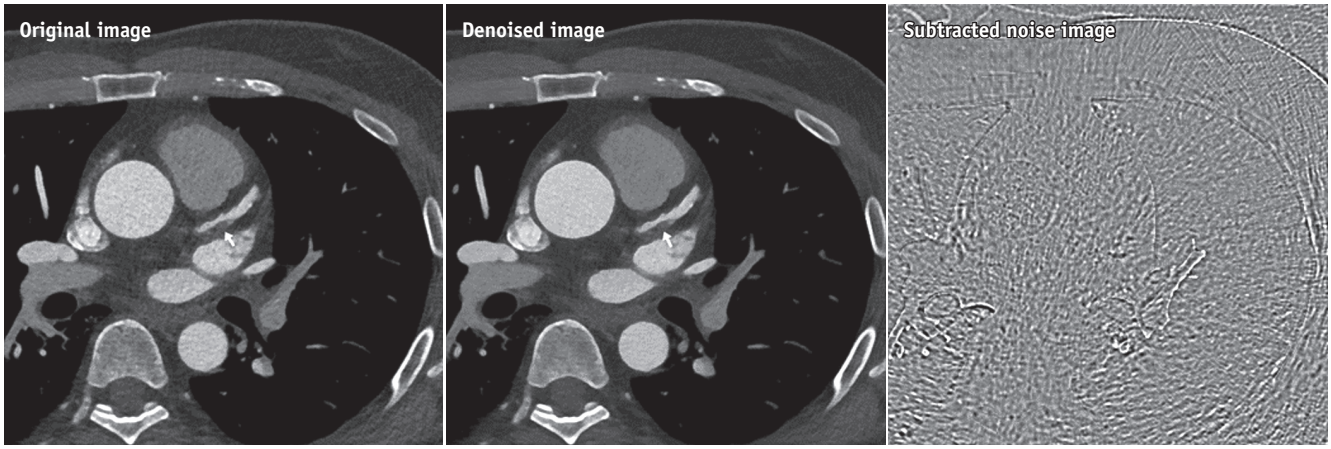

A

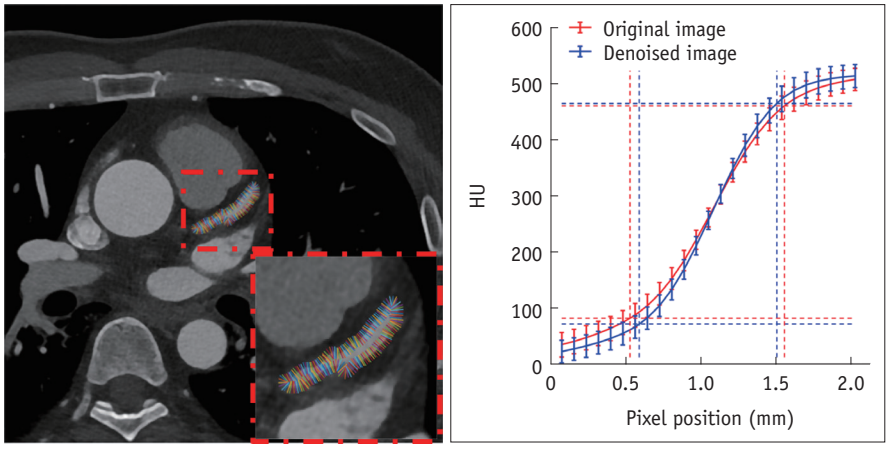

B C

Fig. 4. CT images of 50-year-old male patient.
(A) Original axial CT scan, denoised CT image, and subtracted noise image, **(B)** example of analysis of ERD, and **(C)** graph showing ERDs of original and denoised images. **A.** Denoised image provides sharp contours of vessels because of higher attenuation of vessel lumens and barely perceived image noise. However, stenosis of proximal LAD artery (arrows) is rated to be significant both in original and denoised images. **B.** Multiple short line segments are drawn perpendicular to border of artery with color overlay to calculate ERD. This example is shown on denoised image. **C.** Graph showing comparison of average CT number profiles along line segments of original and denoised images. Average ERD values were 1.0219 and 0.9111 for original and denoised images, respectively. ERD of denoised image is smaller than that of original image, indicating that denoised image is sharper than original image in objective criteria.

Table 3. Segment-Based Diagnostic Accuracy of CCTA according to Original and Denoised Images*

Diagnostic Accuracy	Original	Denoised	*P*
Accuracy	95.1 (988/1039)	95.2 (989/1039)	
Sensitivity	84.3 (145/172)	86.6 (149/172)	0.289
Specificity	97.2 (843/867)	96.9 (840/867)	0.375
PPV	85.8 (145/169)	84.7 (149/176)	0.310
NPV	96.9 (843/870)	97.3 (840/863)	0.170
True positive	145	149	
True negative	843	840	
False positive	24	27	
False negative	27	23	

*Data are presented as percentage (%, number/total number) or number. NPV = negative predictive value, PPV = positive predictive value

deep learning-based denoise algorithms by applying FBP (8, 9, 25-28), the strength of our study is the application of iterative reconstruction-based low-dose CT rather than FBP. We proved that an additional image quality improvement could be achieved by applying the deep learning-based denoising technique to the low-dose CT obtained with iterative reconstruction.

Iterative reconstruction, one of the most widely used noise reduction techniques, has achieved a higher image quality than the FBP by modeling of the image noise with sophisticated mathematical techniques (29-33). However, iterative reconstruction captures the image features from a data-driven formula; it cannot fully achieve the image properties in a personal manner. The strength of a

https://doi.org/10.3348/kjr.2020.0020

deep-learning based denoising technique over iterative reconstruction is personalization because it learns the image features in a completely data-driven way, and it can be easily customized for specific patients. Therefore, adding the denoising technique to iterative reconstruction can potentially improve the image quality further by better utilizing the learned knowledge of a variety of noise patterns caused by the complex interaction between a photon and patient body. In addition, the deep learning-based denoising technique used in our study has vendor-independency; therefore, it can be used by multiple vendors and will be suitable for older CT machines that do not have the modern denoising CT technology.

Our approach of training the deep learning model required only routinely acquired prospective ECG-gated thoracic CTA images and not true low-dose images. Instead, synthetic low-dose noise images were generated by a DICOM-based low-dose simulation tool. Consequently, our deep learning-based denoising technique has the benefit of learning identically matched low- and routine-dose images. In addition, because the proposed method generated a denoised image by subtracting the predicted noise from the original image, the overall image noise decreased without suffering from over-smoothing and loss of details. Our results confirmed a good noise reduction performance of the proposed technique in routine clinical practice.

The deep learning-based denoising technique has a potential application in various clinical settings, such as retrospectively gated cardiac CT scans with ECG-gated tube current modulation that can provide additional information on a reduced dose-phase: functional information such as ventricular volume measurement and multiphase information for coronary arteries. Considering its noise reduction and SNR improvement, this denoising technique may allow a lower radiation dose acquisition protocol. Further studies considering the possibility of reduction in the radiation dose and utilization of the reduced dose-phase in tube current modulation need to be conducted.

This software with deep learning-based denoising technique can be easily used by radiologists. The software runs on a standard personal computer equipped with a graphics processing unit (GPU) card and provides a convenient and user-friendly interface. A user can select and drag a DICOM folder with the mouse and drop it on the software screen; subsequently, the software conducts the denoising process. The software can also send the denoised images to workstation for further processing. The denoising process took less than 1 minute for a data set of 200 images.

In this study, ECG-gated thoracic CTA images were used instead of CCTA images to train deep-learning based denoising software. Our low-dose simulation model consisted of several key steps including the creation of synthetic sinogram, addition of Poisson noise depending on the attenuation of each ray path, application of FBP with the reconstruction kernel function to the noise component sinogram, creation of noise component CT image by intensity scaling after FBP, and addition of the noise component CT image to the input CT image. Because the CCTA images show truncated reconstruction FOVs, the use of a CCTA image as an input leads to the generation of an incorrect synthetic sinogram, which subsequently results in the generation of an inappropriate noise component, which is unable to reflect the correct attenuation of patient body. Therefore, we used CTA images instead of using CCTA images.

Our paper has several limitations. First, the number of subjects in the study population was relatively small, and data were retrospectively collected in a single institution. Second, the patients included in this study belonged to an intermediate or high pre-test probability population. Therefore, the diagnostic accuracy of stenosis, which can be strongly affected by pre-test probability, may have resulted in an overestimation. Third, the significance of the coronary artery stenosis was visually dichotomized without quantitative analysis according to the presence or absence of significant stenosis. Fourth, the CT quantification was performed with only one CT scanner type and limited CT protocols. Further external validation provided by its application to other CT scanners and protocols will be required before the wider applicability of the proposed denoising method can be known. Fifth, the mean body mass index (BMI) of patients examined in this study was 24.65 ± 3.37 kg/m^2, which is smaller than those of average American and European subjects. Further studies are required to determine whether their results also apply to heavier patients. Sixth, despite the occurrence of improvements in objective and subjective image qualities, there were no significant differences in the diagnostic performance regarding stenosis detection between original and denoised images. The original images of our study were acquired on a third generation 192-section dual source CT scanner, which had already been proved to show a good CCTA-related diagnostic accuracy. A limited number of study subjects (82

https://doi.org/10.3348/kjr.2020.0020

Korean Journal of Radiology
KJR

cases) from a single institution and high proportion of low-BMI patients (mean ± SD, 24.65 ± 3.37), which makes it possible to underestimate noise reduction effects, may also the reasons associated with our results. As with our deep learning based denoising software, iterative reconstruction algorithms, which are an alternative to traditional FBP reconstructions, have been proven by various studies to improve objective and subjective image quality. However, few techniques have been shown to improve the diagnostic accuracy more than FBP, at the same radiation dose (34-38). Instead, most studies have demonstrated that low radiation dose techniques enabled by an iterative reconstruction algorithm while maintaining diagnostic accuracy (39-41). Like iterative reconstruction algorithm, although our software did not achieve an improvement in diagnostic accuracy, this technique can be applied in various clinical setting. Our deep learning-based denoising technique has a potential to allow low-radiation-dose acquisition protocol like iterative reconstruction algorithm does (38, 42, 43). The low image noise associated with our technology can encourage reader's confidence and preference towards it in clinical practice. In addition, our deep learning-based denoising technique has vendor-independency. Thus, it can be carried out in older multiple-vendor CT machines, which do not have the modern denoising CT technology. The deep learning-based denoising technique can be useful for imaging patients who are prone to yield noisy images, such as obese patients. Further studies focusing on the possibility of reduction in the radiation dose using a larger population are warranted.

In summary, our study has demonstrated that the proposed denoising technique applied to low-dose CCTA with iterative reconstruction enables image noise reduction and significantly improves the objective and subjective image qualities without over-smoothing. There is a potential for its utilization in routine clinical practice, further radiation dose reduction, and additional functional image achievement in the future.

Supplementary Materials

The Data Supplement is available with this article at https://doi.org/10.3348/kjr.2020.0020.

Conflicts of Interest

Jong-Hyo Kim is the inventor of the technique and a share holder of ClariPI inc.

Other authors have no conflict of interest including financial or consultant, institutional and other relationship in this study.

ORCID iDs

Eun-Ah Park
https://orcid.org/0000-0001-6203-1070
Jung Hee Hong
https://orcid.org/0000-0002-4299-6411
Whal Lee
https://orcid.org/0000-0003-1285-5033
Chulkyun Ahn
https://orcid.org/0000-0003-2919-4892
Jong-Hyo Kim
https://orcid.org/0000-0002-5695-4976

REFERENCES

1. Hamilton-Craig CR, Friedman D, Achenbach S. Cardiac computed tomography—Evidence, limitations and clinical application. *Heart Lung Circ* 2012;21:70-81
2. Task Force Members; Montalescot G, Sechtem U, Achenbach S, Andreotti F, Arden C, Budaj A, et al. 2013 ESC guidelines on the management of stable coronary artery disease: the task force on the management of stable coronary artery disease of the European Society of Cardiology. *Eur Heart J* 2013;34:2949-3003
3. Deseive S, Chen MY, Korosoglou G, Leipsic J, Martuscelli E, Carrascosa P, et al. Prospective randomized trial on radiation dose estimates of CT angiography applying iterative image reconstruction: the PROTECTION V study. *JACC Cardiovasc Imaging* 2015;8:888-896
4. Halliburton SS, Abbara S, Chen MY, Gentry R, Mahesh M, Raff GL, et al. SCCT guidelines on radiation dose and dose-optimization strategies in cardiovascular CT. *J Cardiovasc Comput Tomogr* 2011;5:198-224
5. Hausleiter J, Meyer TS, Martuscelli E, Spagnolo P, Yamamoto H, Carrascosa P, et al. Image quality and radiation exposure with prospectively ECG-triggered axial scanning for coronary CT angiography: the multicenter, multivendor, randomized PROTECTION-III study. *JACC Cardiovasc Imaging* 2012;5:484-493
6. Hirshfeld JW Jr, Ferrari VA, Bengel FM, Bergersen L, Chambers CE, Einstein AJ, et al. 2018 ACC/HRS/NASCI/SCAI/SCCT expert consensus document on optimal use of ionizing radiation in cardiovascular imaging: best practices for safety and effectiveness: a report of the American College of Cardiology task force on expert consensus decision pathways. *J Am Coll Cardiol* 2018;71:e283-e351
7. Stocker TJ, Deseive S, Leipsic J, Hadamitzky M, Chen MY, Rubinshtein R, et al. Reduction in radiation exposure in

cardiovascular computed tomography imaging: results from the PROspective multicenter registry on radiaTion dose Estimates of cardiac CT angIOgraphy iN daily practice in 2017 (PROTECTION VI). *Eur Heart J* 2018;39:3715-3723
8. Chen H, Zhang Y, Kalra MK, Lin F, Chen Y, Liao P, et al. Low-dose CT with a residual encoder-decoder convolutional neural network. *IEEE Trans Med Imaging* 2017;36:2524-2535
9. Kang E, Chang W, Yoo J, Ye JC. Deep convolutional framelet denosing for low-dose CT via wavelet residual network. *IEEE Trans Med Imaging* 2018;37:1358-1369
10. Ahn CK, Jin H, Heo C, Kim JH. *Combined low-dose simulation and deep learning for CT denoising: application of ultra-low-dose cardiac CTA*. In: Schmidt TG, Chen GH, Bosmans H, eds. *Proceedings of SPIE, Volume 10948*. Bellingham: SPIE, 2019
11. Ronneberger O, Fischer P, Brox T. U-net: convolutional networks for biomedical image segmentation. Cornell University, 2015. Available at: https://arxiv.org/abs/1505.04597. Accessed March 8, 2019
12. Ioffe S, Szegedy C. Batch normalization: accelerating deep network training by reducing internal covariate shift [updated Mar 2015]. Cornell University, 2015. Available at: https://arxiv.org/abs/1502.03167. Accessed March 8, 2019
13. Nair V, Hinton GE. *Rectified linear units improve restricted boltzmann machines*. In: Fürnkranz J, Joachims T. *Proceedings of the 27th international conference on international conference on machine learning*. Madison: Omnipress, 2010
14. Kingma DP, Ba J. Adam: a method for stochastic optimization [updated Jan 2017]. Cornell University, 2014. Available at: https://arxiv.org/abs/1412.6980. Accessed March 8, 2019
15. Abadi M, Barham P, Chen J, Chen Z, Davis A, Dean J, et al.; Google Brain. *Tensorflow: a system for large-scale machine learning*. In: USENIX Association, eds. 12th USENIX symposium on operating systems design and implementation (Proceedings of OSDI '16). Berkeley: USENIX Association, 2016:265-283
16. Kim CW, Kim JH. Realistic simulation of reduced-dose CT with noise modeling and sinogram synthesis using DICOM CT images. *Med Phys* 2014;41:011901
17. Mangold S, Wichmann JL, Schoepf UJ, Caruso D, Tesche C, Steinberg DH, et al. Diagnostic accuracy of coronary CT angiography using 3rd-generation dual-source CT and automated tube voltage selection: clinical application in a non-obese and obese patient population. *Eur Radiol* 2017;27:2298-2308
18. Achenbach S, Paul JF, Laurent F, Becker HC, Rengo M, Caudron J, et al. Comparative assessment of image quality for coronary CT angiography with iobitridol and two contrast agents with higher iodine concentrations: iopromide and iomeprol. A multicentre randomized double-blind trial. *Eur Radiol* 2017;27:821-830
19. Yi Y, Wu W, Lin L, Zhang HZ, Qian H, Shen ZJ, et al. Single-phase coronary artery CT angiography extracted from stress dynamic myocardial CT perfusion on third-generation dual-source CT: validation by coronary angiography. *Int J Cardiol* 2018;269:343-349
20. Smith SW. *Digital signal processors*. In: Smith SW, ed. *The scientist and engineer's guide to diginal signal processing*. San Diego: California Technical Publishing, 1997:503-534
21. Leipsic J, Nguyen G, Brown J, Sin D, Mayo JR. A prospective evaluation of dose reduction and image quality in chest CT using adaptive statistical iterative reconstruction. *AJR Am J Roentgenol* 2010;195:1095-1099
22. Marin D, Nelson RC, Schindera ST, Richard S, Youngblood RS, Yoshizumi TT, et al. Low-tube-voltage, high-tube-current multidetector abdominal CT: improved image quality and decreased radiation dose with adaptive statistical iterative reconstruction algorithm—Initial clinical experience. *Radiology* 2010;254:145-153
23. Chun EJ, Lee W, Choi YH, Koo BK, Choi SI, Jae HJ, et al. Effects of nitroglycerin on the diagnostic accuracy of electrocardiogram-gated coronary computed tomography angiography. *J Comput Assist Tomogr* 2008;32:86-92
24. Moskowitz CS, Pepe MS. Comparing the predictive values of diagnostic tests: sample size and analysis for paired study designs. *Clin Trials* 2006;3:272-279
25. Kang E, Koo HJ, Yang DH, Seo JB, Ye JC. Cycle-consistent adversarial denoising network for multiphase coronary CT angiography. *Med Phys* 2019;46:550-562
26. Ahn C, Heo C, Kim JH. *Combined low-dose simulation and deep learning for CT denoising: application in ultra-low-dose chest CT*. In: Lin F, Fujita H, Kim JH, eds. *International forum on medical imaging in Asia 2019, Volume 11050*. Bellingham: SPIE, 2019
27. Ahn CK, Yang Z, Heo C, Jin H, Park B, Kim JH. *A deep learning-enabled iterative reconstruction of ultra-low-dose CT: Use of synthetic sinogram-based noise simulation technique*. In: Lo JY, Schmidt TG, Chen GH, eds. *Medical imaging 2018: physics of medical imaging, Volume 10573*. Bellingham: SPIE, 2018
28. Yang Q, Yan P, Zhang Y, Yu H, Shi Y, Mou X, et al. Low-dose CT image denoising using a generative adversarial network with wasserstein distance and perceptual loss. *IEEE Trans Med Imaging* 2018;37:1348-1357
29. Hara AK, Paden RG, Silva AC, Kujak JL, Lawder HJ, Pavlicek W. Iterative reconstruction technique for reducing body radiation dose at CT: feasibility study. *AJR Am J Roentgenol* 2009;193:764-771
30. Katsura M, Matsuda I, Akahane M, Sato J, Akai H, Yasaka K, et al. Model-based iterative reconstruction technique for radiation dose reduction in chest CT: comparison with the adaptive statistical iterative reconstruction technique. *Eur Radiol* 2012;22:1613-1623
31. Li T, Tang T, Yang L, Zhang X, Li X, Luo C. Coronary CT angiography with knowledge-based iterative model reconstruction for assessing coronary arteries and non-calcified predominant plaques. *Korean J Radiol* 2019;20:729-738
32. Park C, Choo KS, Kim JH, Nam KJ, Lee JW, Kim JY. Image

https://doi.org/10.3348/kjr.2020.0020

quality and radiation dose in CT venography using model-based iterative reconstruction at 80 kVp versus adaptive statistical iterative reconstruction-V at 70 kVp. *Korean J Radiol* 2019;20:1167-1175
33. Lim WH, Choi YH, Park JE, Cho YJ, Lee S, Cheon JE, et al. Application of vendor-neutral iterative reconstruction technique to pediatric abdominal computed tomography. *Korean J Radiol* 2019;20:1358-1367
34. Yoo RE, Park EA, Lee W, Shim H, Kim YK, Chung JW, et al. Image quality of adaptive iterative dose reduction 3D of coronary CT angiography of 640-slice CT: comparison with filtered back-projection. *Int J Cardiovasc Imaging* 2013;29:669-676
35. Wang R, Schoepf UJ, Wu R, Nance JW Jr, Lv B, Yang H, et al. Diagnostic accuracy of coronary CT angiography: comparison of filtered back projection and iterative reconstruction with different strengths. *J Comput Assist Tomogr* 2014;38:179-184
36. Precht H, Gerke O, Thygesen J, Egstrup K, Auscher S, Waaler D, et al. Image quality in coronary computed tomography angiography: influence of adaptive statistical iterative reconstruction at various radiation dose levels. *Acta Radiol* 2018;59:1194-1202
37. Fuchs TA, Fiechter M, Gebhard C, Stehli J, Ghadri JR, Kazakauskaite E, et al. CT coronary angiography: impact of adapted statistical iterative reconstruction (ASIR) on coronary stenosis and plaque composition analysis. *Int J Cardiovasc Imaging* 2013;29:719-724
38. Leipsic J, Labounty TM, Heilbron B, Min JK, Mancini GB, Lin FY, et al. Adaptive statistical iterative reconstruction: assessment of image noise and image quality in coronary CT angiography. *AJR Am J Roentgenol* 2010;195:649-654
39. Yin WH, Lu B, Li N, Han L, Hou ZH, Wu RZ, et al. Iterative reconstruction to preserve image quality and diagnostic accuracy at reduced radiation dose in coronary CT angiography: an intraindividual comparison. *JACC Cardiovasc Imaging* 2013;6:1239-1249
40. Moscariello A, Takx RA, Schoepf UJ, Renker M, Zwerner PL, O'Brien TX, et al. Coronary CT angiography: image quality, diagnostic accuracy, and potential for radiation dose reduction using a novel iterative image reconstruction technique-comparison with traditional filtered back projection. *Eur Radiol* 2011;21:2130-2138
41. Leipsic J, Labounty TM, Heilbron B, Min JK, Mancini GB, Lin FY, et al. Estimated radiation dose reduction using adaptive statistical iterative reconstruction in coronary CT angiography: the ERASIR study. *AJR Am J Roentgenol* 2010;195:655-660
42. Renker M, Ramachandra A, Schoepf UJ, Raupach R, Apfaltrer P, Rowe GW, et al. Iterative image reconstruction techniques: applications for cardiac CT. *J Cardiovasc Comput Tomogr* 2011;5:225-230
43. Song JS, Choi EJ, Kim EY, Kwak HS, Han YM. Attenuation-based automatic kilovoltage selection and sinogram-affirmed iterative reconstruction: effects on radiation exposure and image quality of portal-phase liver CT. *Korean J Radiol* 2015;16:69-79
44. Deak PD, Smal Y, Kalender WA. Multisection CT protocols: sex- and age-specific conversion factors used to determine effective dose from dose-length product. *Radiology* 2010;257:158-166

 https://doi.org/10.3348/kjr.2020.0020